Journal of Molecular Catalysis A: Chemical 310 (2009) 113–120

Contents lists available at ScienceDirect

Journal of Molecular Catalysis A: Chemical

journal homepage: www.elsevier.com/locate/molcata

Interactions of phosphorous molecules with the acid sites of H-Beta zeolite: Insights from solid-state NMR techniques and theoretical calculations

Jing Guan, Xiujie Li, Gang Yang, Weiping Zhang, Xianchun Liu, Xiuwen Han, Xinhe Bao*

State Key Laboratory of Catalysis, Dalian Institute of Chemical Physics, Chinese Academy of Sciences, Dalian 116023, People's Republic of China

ARTICLE INFO

Article history:
Received 12 April 2009
Received in revised form 26 May 2009
Accepted 4 June 2009
Available online 10 June 2009

Keywords:
Solid-state NMR technique
Theoretical calculations
Brønsted acids
Lewis acids
Probe molecule

ABSTRACT

The local structures of various Brønsted and Lewis acid sites in H-Beta zeolite were resolved with the combined ^{31}P MAS NMR, ^{31}P–^{27}Al TRAPDOR NMR experiments and theoretical calculations at different levels. In addition, the interacting mechanisms of these acid sites with probe molecules such as trimethylphosphine (TMP) and trimethylphosphine oxide (TMPO) were clarified, which greatly aids the understanding of acid catalysis. Owing to the narrow chemical shift range and close Brønsted acid strengths, only an average resonance at −4.5 ppm was observed in TMP adsorbed H-Beta zeolite, consistent with the calculated data of acidities (substitution energies and proton affinities), geometries, adsorption energies as well as ^{31}P chemical shifts. However, two types of Brønsted acids were distinguished by TMPO, and the HF/DZVP2 (MP2/DZVP2) chemical shifts were calculated at 68.1 (69.5) and 69.7–72.1 (71.7–74.9) ppm, respectively. Two types of Lewis acids were identified at −32.0 and −47.0 ppm with the latter exhibiting strong ^{31}P–^{27}Al TRAPDOR effects. With theoretical calculations, these two peaks were attributed to the extra-lattice oxo-$AlOH^{2+}$ species and the three-fold coordinated lattice-Al, extra-framework $Al(OH)_3$, oxo-AlO^+ species, respectively. The peak at −60.0 ppm was conventionally assigned to the TMP physisorption, but the calculations indicated that the EFAL monovalent $Al(OH)_2^+$ species coordinating with two lattice-O atoms near the framework Al atom can contribute to it as well.

1. Introduction

Owing to the strong acidity and peculiar pore systems, H-Beta zeolite has aroused a wide interest since its discovery in 1988 [1]. It plays a more and more important role in today's heterogeneous catalysis. Recently, our laboratory has reported that the proper acidity may be advantageous for the cross-metathesis of ethylene and 2-butylene to produce propylene, with the Mo/H-Beta and Al_2O_3 composites used as the catalysts [2]. Many spectroscopic techniques were applied to determine the types, concentrations and acid strengths of H-Beta zeolite [3–5]. It is well-known that the Brønsted acid sites are caused by the bridging hydroxyl protons in the vicinity of the tetrahedrally coordinated lattice-Al atoms, which are the active sites for various chemical reactions such as alkylation and cracking [6–8]. However, the acid strengths in H-Beta zeolite may differ from site to site, which are still unclear to us. As to the Lewis acids, the controversies are ubiquitous to all the found zeolites, including H-Beta. A number of extra-framework Al (EFAL) species were suggested to be responsible for the Lewis acidities in zeolites [9–12]. On the other hand, others attributed the Lewis acidities to the presence of three-fold coordinated lattice-Al centers [13–15]. Compared with other zeolites, H-Beta zeolite possesses unique acid properties that are related to the local defects, where the lattice-T atoms are partially coordinated [16].

Among the numerous spectroscopic techniques, solid-state NMR is probably the most powerful to characterize the acid sites of porous materials, including zeolites. Because the P element has 100% natural abundance and 1/2 spin nucleus, trimethylphosphine (TMP) and trimethylphosphine oxide (TMPO) have often been used as probe molecules. The ^{31}P MAS NMR spectra were widely employed to discriminate the Brønsted and Lewis acid sites of H-form zeolites [17–23]. However, the information about the local structures of Brønsted and Lewis acid sites in H-Beta zeolite is severely lacking, which was attempted in this work. First of all, the positions of the bridging hydroxyl protons have to be determined, which were done with the two-layer ONIOM scheme. On such basis, the various Brønsted and Lewis acid sites in H-Beta zeolite were clarified with density functional theory (DFT) and Hartree-Fork (HF) calculations as well as combined ^{31}P MAS NMR and ^{31}P–^{27}Al TRAPDOR experiments. Through the present studies, the interaction mechanisms of the acid sites with probe molecules were understood, which greatly helps us to understand the acid properties of zeolites and acid catalysis.

* Corresponding author. Tel.: +86 411 84686637; fax: +86 411 84694447.
E-mail address: xhbao@dicp.ac.cn (X. Bao).

1381-1169/$ – see front matter © 2009 Published by Elsevier B.V.
doi:10.1016/j.molcata.2009.06.005

2. Experimental

The samples of H-Beta zeolite with the Si/Al ratio of 15 were kindly provided by Fushun Petroleum Company, China. The samples were dehydrated at 400 °C under the pressure below 10^{-2} Pa for 20 h. Adsorption of TMP was performed by exposing the dehydrated sample to saturated TMP (99%, Acros) vapor at room temperature for 1 h. The samples with adsorbed TMP molecules were degassed for 0.5 h at 20, 50, 60, 70 and 80 °C, respectively. In this way, the zeolite samples were ready for the NMR experiments by packing in a glove box into the ZrO_2 rotors with tightly fitting Kel-F caps.

All the MAS NMR spectra were recorded on Varian Infinityplus-400 spectrometer using a Chemagnetic triple-resonance 7.5 mm probe or double-resonance 4 mm probe. The ^{31}P MAS NMR spectra were acquired with high-power decoupling, a repetition time of 4 s, a $\pi/4$ pulse length of 2 μs and a spinning speed of 10 kHz. The ^{31}P NMR chemical shifts were referenced to 85% H_3PO_4. The ^{31}P–^{27}Al TRAPDOR experiments were carried out with and without Al irradiations during one of the two echo periods, τ, which equals multiples of the rotor period [24]. An Al radio-frequency (rf) field amplitude of 60 kHz and a spinning speed of 4 kHz were used for the TRAPDOR NMR experiments.

3. Computational section

3.1. Cluster models

As in our previous works [25,26], the Beta zeolite models were taken from the framework structure of polymorph A [1]. There are nine distinct T sites in Beta zeolite and they can be grouped into three topographical categories: T1 and T2 are associated with one four-membered ring, T3, T4, T5 and T6 fall at the crossings of two four-membered rings, and T7, T8 and T9 have no relations with four-membered rings [27]. The T sites of the same group share quite similar geometries, and therefore T1, T6 and T8 were chosen to interact with TMP and TMPO probe molecules.

Prior to the studies on the interactions with probe molecules, the acid protons of the T sites in H-Beta zeolite have to be located. As shown in Fig. 1, the cluster models with 32 T sites ($AlSi_{31}O_{44}H_{41}$) were used for this purpose, where the active sites were represented with $(HO)_3Al–O(H)–Si(OH)_3$ while the rest considered as the environment. On the basis of the determined locations of the acid protons, a series of 9 T cluster models were used to study the interactions between the Brønsted acid sites of H-Beta zeolite and probe molecules. To retain the integrity of the zeolite structures, the active sites of the 32 T cluster models, the central $O_3Si–OH–AlO_3$ fragments of the 9 T cluster models as well as the probe molecules were allowed to fully relax whereas the others were fixed at their crystallographic positions. The terminal Si and O atoms were saturated with hydrogen atoms, which were oriented along the bond vectors of what would have been the next zeolite lattice atoms. The terminal Si–H and O–H distances were set to 1.500 and 1.000 Å, respectively.

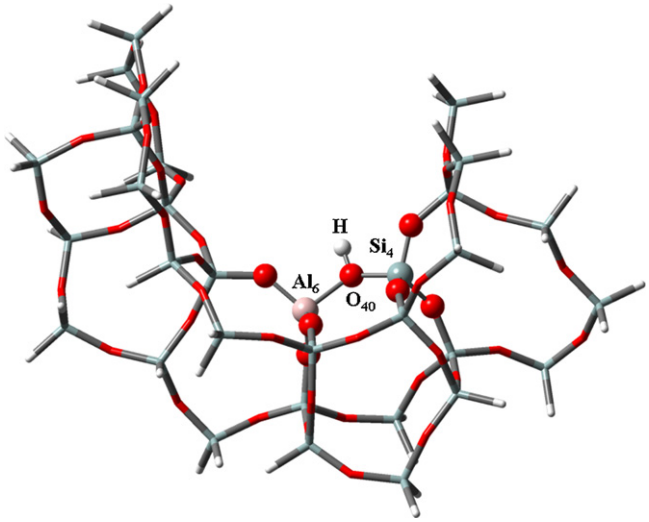

Fig. 1. The cluster models of zeolite H-Beta for the ONIOM approach, the ball and sticks represent the active sites and treated with B3LYP/6-31G (d, p) method, the rest are the environmental atoms and treated with HF/3-21G method.

The interactions of Lewis acid sites with probe molecules were studied as well. On the basis of previous literatures [9–15], three types of Lewis acid sites were constructed: (I) Three-fold coordinated Al species, which are connected with three lattice-O atoms. It was caused by the hydrolysis of Si–O–Al links. To the best of our knowledge, this is the most common and facile Lewis acid sites in zeolites [16]. The Al_5, Al_8 and Al_1 sites with this type of Lewis acids were designated to be LI_1, LI_2 and LI_3, respectively. The further hydrolysis of Si–O–Al links may lead to the Al–OH species, where two lattice-O atoms and one hydroxyl group (O–H) are bonded to the Al atom. The Al–OH species was tentatively created for the Al_5 site (referred as LI_4), but the agreements of the calculated ^{31}P chemical shift with the NMR experimental data are not satisfactory, see the details in Section 4. Accordingly, it is not likely to form the Al–OH species in H-Beta zeolite, which was also observed in our previous studies of TS-1 zeolite [28]. (II) Extra-framework Al species. Under severe conditions, some of the Al atoms are expelled out of lattices and form the EFAL monovalent AlO^+ and $Al(OH)_2^+$ cations [29], which were referred to LII_1 and LII_2, respectively. (III) Oxo-Al species that have synergistic interplays with the Brønsted acid sites such as $Al(OH)_3$, AlO^+, $AlOH^{2+}$ and $Al(OH)_2^+$ (referred as $LIII_1$, $LIII_2$, $LIII_3$ and $LIII_4$, respectively) [30,31]. These oxo-Al species were coordinated with the O atoms at the lattice Al_5 atoms. Some other lattice-Al atoms were introduced in order to compensate the positive charges caused by the oxo-Al species. In all the clusters of Lewis acid sites, the central Al atoms of the Beta zeolites were surrounded by two shells of Si atoms. The treatments of boundary atoms were identical to those of the above Brønsted acid sites.

3.2. Theoretical methods

All the calculations were performed using GAUSSIAN98 software package [32]. The two-layer ONIOM scheme developed by Maseras and Morokuma [33] was used to calculate the 32 T cluster models for determining the acidic proton positions. The active sites and the environmental atoms defined in Section 3.1 were described with the B3LYP/6-31G (d, p) and HF/3-21G levels of theory, respectively. The structures of probe molecules adsorbed at the 9 T cluster models of Brønsted acid sites were optimized at B3LYP/TZVP level of theory. It is known that the precise predictions of the ^{31}P NMR parameters are difficult for the current computational techniques [34,35]. The HF/DZVP2 method was employed by Zheng et al. to predict the ^{31}P chemical shifts for TMPO adsorbed on the acid sties of H-MCM-22 zeolite, which were found to be in good agreement with the NMR experimental data [36]. Hence, the ^{31}P NMR isotropic chemical shifts for the TMP and TMPO adsorption complexes on the Brønsted acid sties of H-Beta zeolite were calculated at HF/DZVP2 level of theory and referenced to those of liquid phase TMP (−62 ppm) and crystalline TMPO (39 ppm), respectively. The NMR parameters were calculated using the gauge-independent atomic orbital (GIAO) method [37,38]. The structures of TMP interacting with Lewis acid sites of H-Beta were obtained at B3LYP/6-31G (d, p) level of theory. The ^{31}P isotropic chemical shifts were calculated at both B3LYP/6-31G (d, p) and HF/DZVP2 levels and referenced to that of liquid phase TMP (−62 ppm). The

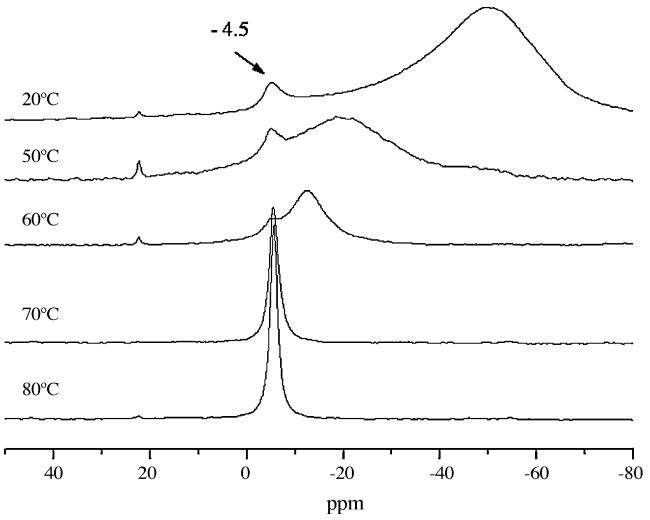

Fig. 2. The ^{31}P MAS NMR spectra of TMP/H-Beta sample with different degassing temperature.

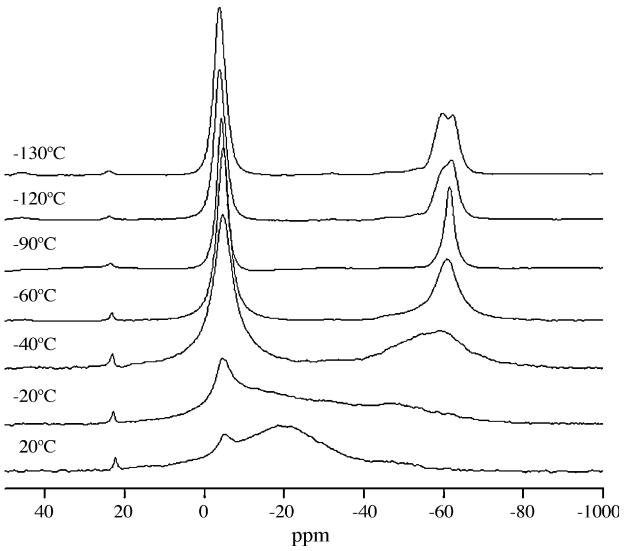

Fig. 3. The variable-temperature ^{31}P MAS NMR spectra of the TMP/H-Beta sample degassed at 50 °C with a spinning speed of 8 kHz.

calculated magnetic shielding constants (σ_{cal}) were converted to chemical shifts (δ_{cal}) by the following equation:

$$\delta_{cal} = \sigma_{ref} - \sigma_{cal} + \delta_{ref}$$

where σ_{ref} is the nuclear magnetic shielding constants for the reference compound at the same level of theory, δ_{ref} is the experimental chemical shift for the reference compound.

4. Results and discussion

4.1. ^{31}P MAS NMR spectra

The ^{31}P MAS NMR spectra of TMP adsorbed H-Beta zeolite samples degassed at different temperatures are shown in Fig. 2. It is found that at room temperature, the adsorbed TMP molecules at different Brønsted acid sites undergo fast exchanges. Only a single signal at around −4.5 ppm is observed, corresponding to the formation of the $TMPH^+$ species [17–20]. The broad peak at 0 to −60 ppm may be caused by the fast exchanges between the Lewis-bound TMP molecules, the physisorbed TMP and the protonated $TMPH^+$ ions. The small resonance at 24.0 ppm is usually assigned to the $P(CH_3)_4^+$ species, arising from the reactions of TMP adsorbed on the Brønsted acid sites with excess TMP molecules in the gas phase [39]. With the increase of degassing temperatures, the broad peak at 0 to −60 ppm gradually shifts down-field and decreases in intensity. It indicates that the weakly bound TMP molecules are gradually desorbed from H-Beta zeolite. As the temperature approaches 80 °C, this peak disappears completely and only the resonance at −4.5 ppm is still present.

Variable-temperature ^{31}P MAS NMR experiments are carried out on the TMP adsorbed H-Beta zeolite, with the spectra shown in Fig. 3. Upon the decrease of temperatures, the signal responsible for TMP adsorption at the Brønsted acid sites (−4.5 ppm) becomes stronger. When the temperature is lowered to −40 °C, two ^{31}P NMR peaks are resolved at −4.5 and −55.0 ppm due to the slow exchanges of TMP molecules at different acid sites. The further decrease of temperatures causes the high-field shift of the resonance at −55.0 ppm and the narrowing of the peak. The signal at high-field is broadened and split into two peaks when the temperature is lower than −120 °C.

As the enlarged Fig. 4a indicates, two small resonances at −32.0 and −47.0 ppm are present for the TMP adsorbed H-Beta zeolite samples at −100 °C together with the major resonance at

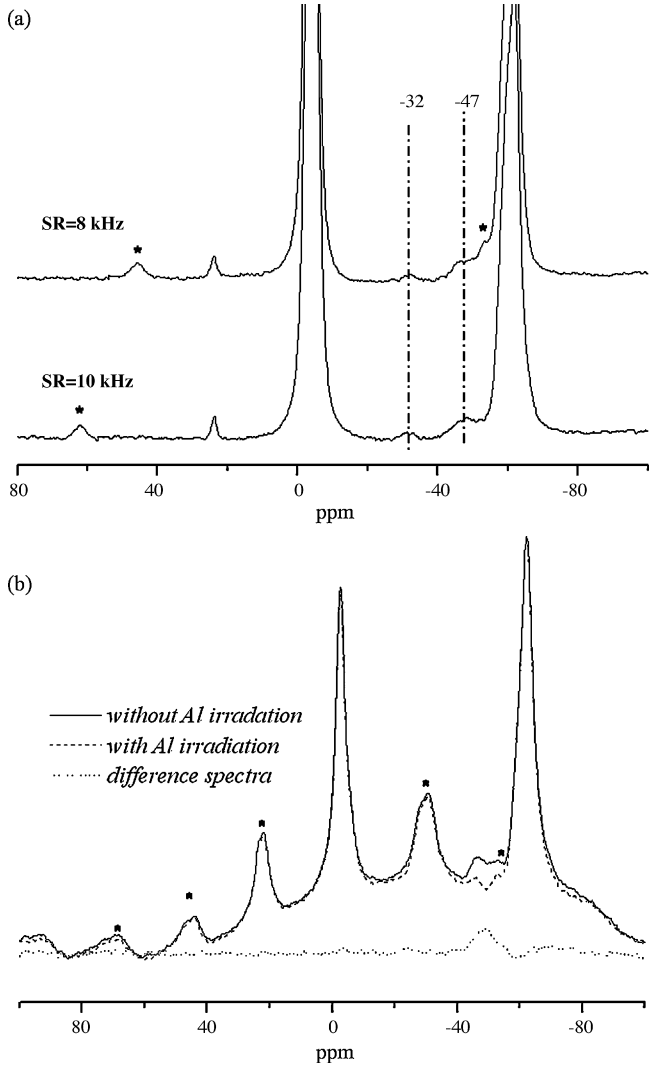

Fig. 4. The NMR spectra of the TMP/H-Beta sample at −100 °C. The samples were pre-degassed at 50 °C and the asterisks denoted the spinning side bands. (a) ^{31}P MAS NMR and (b) ^{31}P–^{27}Al TRAPDOR.

−60.0 ppm. These resonances at −32.0 and −47.0 ppm are assigned to the TMP species bound to the Lewis acid sites [17–20]. Earlier studies suggested that the resonance at −60 ppm is caused by the physisorbed TMP molecules [17–20]. The ^{31}P MAS NMR experiments are also performed with a spinning speed of 8 kHz instead of 10 kHz. It confirms that the resonances at −32.0 and −47.0 ppm are not caused by the side bands but related with the adsorbed TMP species. The ^{31}P–^{27}Al TRAPDOR spectra acquired at the same temperature (−100 °C) are given in Fig. 4b, which provides the information of the proximity degrees of TMP molecules and Al atoms. The echo intensity of the resonance at −47.0 ppm decreases considerably when ^{27}Al on-resonance irradiation is applied, while only negligible influences are observed for the resonances at −4.5, −32.0 and −60.0 ppm. Accordingly, only the TMP molecules responsible for the resonance at −47.0 ppm are in close proximity to the Al atoms.

4.2. Theoretical determinations of the locations of acid protons

In zeolites, one unit of negative charge is created when a lattice Si atom is replaced by an Al atom. Protons are usually used to compensate the negative charges; however, all the four unequivalent O atoms bonded to the Al atoms may accommodate the protons. The O atoms that are inaccessible to probe molecules are excluded from calculations such as the Al_1–OH–Si_2 link. The relative substitution energies for the Al_1, Al_6 and Al_8 sites in H-Beta zeolite are calculated and listed in Table 1, ranging within 9.0 kcal mol^{-1}. The substitution energies increase in the order of Al_6–OH–Si_4 < Al_6–OH–Si_8 < Al_1–OH–Si_3 < Al_8–OH–Si_3 < Al_8–OH–Si_6 < Al_6–OH–Si_5. That is, the Al_6–OH–Si_4 link is the most preferential location. However, the energy differences of different Al sites are not more than 3.3 kcal mol^{-1}, with the acid protons at the most stable Al–OH–Si links. It indicates that all these T sites are possibly occupied by Al atoms if the substitution processes in Beta zeolite are thermodynamically controlled. Fajula and co-workers [40] also investigated the (Al, H)/Si substitutions in H-Beta zeolite using pentameric clusters and found that the relative substitution energies were within a narrow range (1.4 kcal mol^{-1}). In the following calculations of the interactions with probe molecules, three representative acid sites of Al_1–OH–Si_3, Al_6–OH–Si_4 and Al_8–OH–Si_3 are chosen, since these Al–OH–Si links have the lowest substitution energies and therefore are most advantageous for the positions of acid protons.

Besides substitution energies, proton affinity (PA) is also used to measure the acid strengths of different T sites. The PA values can be obtained by calculating the energy differences between the H-form and deprotonated cluster models. The smaller the PA values, the stronger the acidities will be. The PA values using the ONIOM scheme are calculated to be 301.2, 297.1 and 296.1 kcal mol^{-1} for Al_1–OH–Si_3, Al_6–OH–Si_4 and Al_8–OH–Si_3 links, respectively. It can be found that the acid strengths of different T sites in H-Beta zeolite are close to each other.

Table 1
The relative substitution energies (ΔE_{rel})[a] and proton affinities (PA) for the different Al–OH–Si links in H-Beta zeolite.

	ΔE_{rel} (kcal mol^{-1})	PA (kcal mol^{-1})
Al_6–OH–Si_4	0.00	297.1
Al_6–OH–Si_8	1.30	
Al_6–OH–Si_5	8.72	
Al_1–OH–Si_3	2.17	301.2
Al_8–OH–Si_3	3.23	296.1
Al_8–OH–Si_6	4.46	

[a] The substitution energy was referenced to that of the Al_6–OH–Si_4 link.

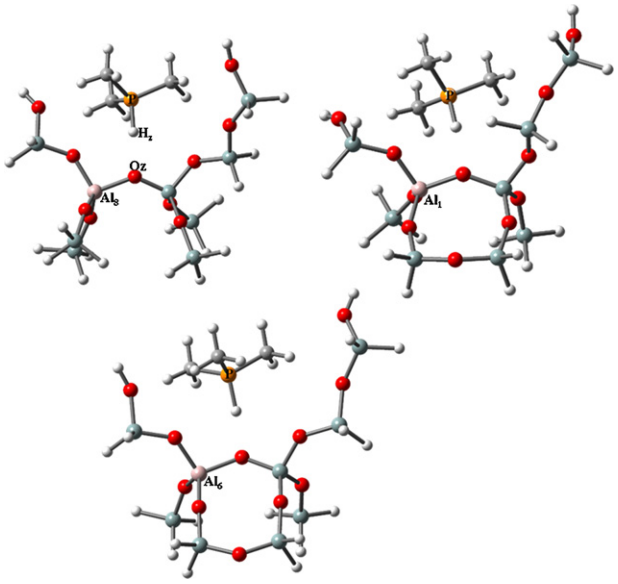

Fig. 5. The B3LYP/TZVP optimized geometries for TMP adsorbed on the different Brønsted acid sites of H-Beta zeolite.

4.3. Interactions of Brønsted acid sites with probe molecules

4.3.1. TMP as the probe molecule

The optimized structures of TMP bound to the Brønsted acid sites of H-Beta are shown in Fig. 5, with the important geometrical parameters and the adsorption energies given in Table 2. The O_z–H_z bond length, about 0.970 Å in the bare cluster of H-Beta, is elongated to 1.782 (Al_6–O–Si_4), 1.842 (Al_8–O–Si_3) and 1.874 Å (Al_1–O–Si_3) in the adsorption complexes, and the forming P–H_z bond distances are 1.421, 1.417 and 1.414 Å, respectively. It is found that for all the Brønsted acid sites, the protons have been transferred to the adsorbed TMP molecules, thus generating the TMPH$^+$ ions. The sequence of acid strengths increases as Al_6–OH–Si_4 < Al_8–OH–Si_3 < Al_1–OH–Si_3, identical to those of the increase of the O_z–H_z distances and the decrease of the P–H_z distances. Generally, the stronger the Brønsted acidity is, the stronger the interaction between the adsorbed TMP molecule and the acid site. However, the adsorption energy differences are small with a maximum value of 1.5 kcal mol^{-1}, suggesting that the acid strengths of the three acid sites in H-Beta zeolite are close to each other. It is in agreement with the above results of substitution energies and proton affinities (PA).

The ^{31}P isotropic chemical shifts for TMP attached to the different Brønsted acid sites are calculated at HF/DZVP2 level of theory [36]. As the data in Table 2 shows, the ^{31}P chemical shifts are predicted at 0.9, 0.7 and −0.5 ppm for Al_6, Al_1 and Al_8 sites, respectively, in reasonable agreement with the experimental value at −4.5 ppm. As expected, the calculated chemical shifts change within a small range of 1.4 ppm, consistent with the experimental observation of an average ^{31}P chemical shift. Owing to the narrow ^{31}P chemical shift range (ca. 3 ppm) of the TMPH$^+$ complexes and the close acid

Table 2
The B3LYP/TZVP geometries and adsorption energies (E_{ads}) for TMP adsorbed on the acid sites of H-Beta zeolite as well as the ^{31}P chemical shifts obtained at HF/DZVP2 level of theory (δ_{cal}) and from ^{31}P MAS NMR experiments (δ_{exp}).

	O_z–H_z (Å)	P–H_z (Å)	E_{ads} (kcal mol^{-1})	δ_{cal} (ppm)	δ_{exp} (ppm)
Al_6–OH–Si_4	1.782	1.421	−20.9	0.9	−4.5
Al_8–OH–Si_3	1.842	1.417	−19.4	−0.5	
Al_1–OH–Si_3	1.874	1.414	−19.9	0.7	

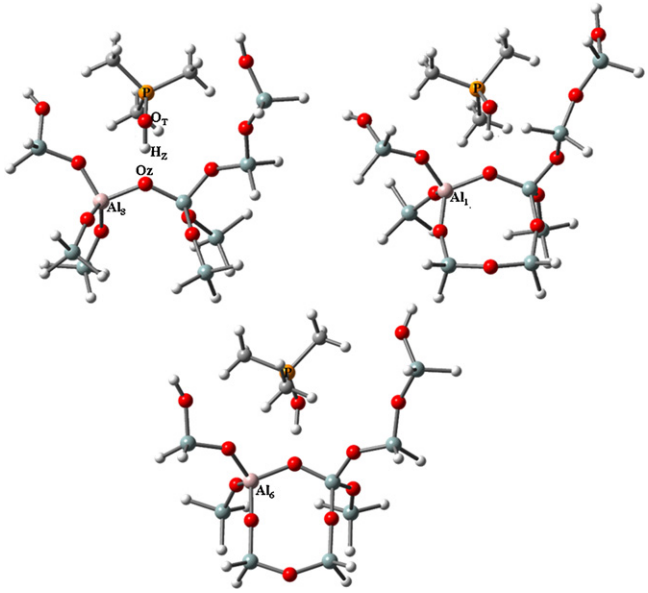

Fig. 6. The B3LYP/TZVP optimized geometries for TMPO adsorbed on the different Brønsted acid sites of H-Beta zeolite.

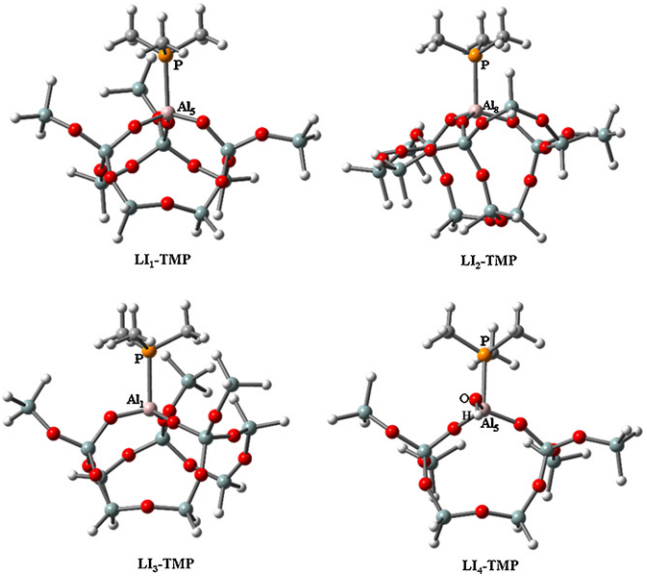

Fig. 7. The B3LYP/6-31G (d, p) optimized geometries for TMP adsorbed on the three-fold coordinated Al species (LI_1, LI_2, LI_3, LI_4) of H-Beta zeolite.

strengths of the different T sites, TMP underwent fast exchanges between the heterogeneously distributed Brønsted acid sites on the experimental NMR time scale. Hence, the ^{31}P MAS NMR technique with adsorbed TMP may not accurately reflect the subtle differences of the acid strengths in zeolites.

4.3.2. TMPO as the probe molecule

Because the ^{31}P nucleus in TMPO has a wider chemical shift range (>300 ppm) than that in TMP, TMPO has advantages for characterizations of Brønsted acidity. As shown by Kao et al. [17], the proton decoupled ^{31}P MAS NMR spectra of TMPO/H-Beta zeolite displayed multiple resonances in the range of 45–90 ppm. The chemical shifts at 71.3 and 67.3 ppm were ascribed to the protonated TMPO species ($TMPOH^+$), which were caused by two different types of Brønsted acid sites.

The optimized structures of TMPO adsorption at the Brønsted acid sites are shown in Fig. 6, with the geometrical parameters and adsorption energies given in Table 3. With the adsorption of TMPO, the O_z–H_z distances are elongated to 1.432, 1.426 and 1.404 Å for Al_1, Al_8 and Al_6 sites, respectively; while the O_T–H_z distances are all optimized at ca. 1.06 Å, indicating that the acid protons are transferred to the adsorbed TMPO molecules and form the $TMPOH^+$ ions. As the O_z–H_z distances indicate, the acid strengths decrease in the order of Al_1–OH–Si_3 > Al_8–OH–Si_3 > Al_6–OH–Si_4, exactly the same as that of TMP adsorption discussed above. The corresponding adsorption energies are calculated at −25.8, −25.7 and −27.8 kcal mol^{-1}, respectively.

For TMPO adsorbed on the acid sites of H-Beta zeolite, the ^{31}P isotropic chemical shifts at HF/DZVP2 level are calculated to be 72.1, 69.7 and 68.1 ppm for Al_1, Al_6 and Al_8 sites, respectively (Table 3), very close to the experimental values at about 70.0 ppm [17]. The down-field signal at 71.3 ppm in the ^{31}P MAS NMR spectra can be attributed to TMPO adsorbed on the Al_1 (72.1 ppm) and Al_6 (69.7 ppm) sites, and the signal at 67.3 ppm corresponds to TMPO adsorbed on the Al_8 (68.1 ppm) site. The classification the acid sites into two types correlates with the structural features. From Fig. 6 it is found that both Al_6 and Al_1 sites have one four-membered ring associated with the Brønsted acid centers, whereas no four-membered ring is present for the Al_8 site. Furthermore, during the adsorption processes, the resulting O–H bond causes the transferring of electron clouds from the TMPO O atom to the electron deficient acid site, which can be reflected from the observance of the ^{31}P chemical shift. Accordingly, the stronger acidity of the Al_1 site leads to a larger down-field shift of the ^{31}P signal, consistent with the geometric analysis discussed above.

Zheng et al. [41] calculated a series of ^{31}P NMR chemical shifts for TMPO adsorption on the Brønsted acid sites of zeolites and derived a correlation function between the MP2 and RHF data: $\delta_{MP2} = [1.327(\pm 0.03710) \times \delta_{HF} - 20.811\ (\pm 2.617)]$. Accordingly, the MP2/DZVP2 chemical shifts are obtained at 74.9, 71.7 and 69.5 ppm for the Al_1, Al_6 and Al_8 sites, respectively. It can be found that the δ_{MP2} values are in good agreement with those of δ_{HF}.

4.4. Interactions of Lewis acid sites with probe molecules

According to the variable-temperature ^{31}P MAS NMR and ^{31}P–^{27}Al TRAPDOR results discussed above, at least three different Lewis acid sites are proposed in H-Beta zeolite, with the details given in Section 3.1. The optimized geometries are shown in Figs. 7–10. For all the structures of the three-fold coordinated Al species (Fig. 7), the Al atoms adopt the tetrahedral coordination when interacting with TMP. The LI_1, LI_2 and LI_3 clusters possess

Table 3
The B3LYP/TZVP geometries and adsorption energies (E_{ads}) for TMPO adsorbed on the acid sites of H-Beta zeolite as well as the ^{31}P chemical shifts obtained at HF/DZVP2 level of theory (δ_{cal}) and from ^{31}P MAS NMR experiments (δ_{exp}).

	O_z–H_z (Å)	O_T–H_z (Å)	O_T–P(Å)	E_{ads} (kcal mol^{-1})	δ_{cal} (ppm)	δ_{exp} (ppm)
Al_8–O–Si_3	1.426	1.057	1.563	−25.7	68.1 (69.5)[a]	67.3
Al_6–O–Si_4	1.404	1.066	1.564	−27.8	69.7 (71.7)	71.3
Al_1–O–Si_3	1.432	1.060	1.565	−25.8	72.1 (74.9)	

[a] The second-order Møller-Plesset (MP2) chemical shift predicted by restricted Hartree-Fock (RHF) calculation using the linear correlation: $\delta_{MP2} = [1.327(\pm 0.03710) \times \delta_{HF} - 20.811\ (\pm 2.617)]$ in reference [40].

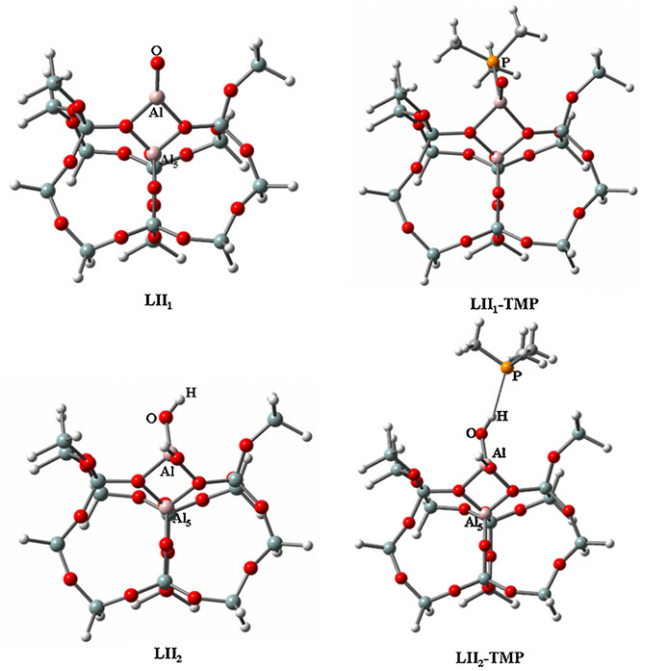

Fig. 8. The B3LYP/6-31G (d, p) optimized geometries for the extra-lattice AlO^+ (LII_1) and $Al(OH)_2^+$ (LII_2) species of H-Beta zeolite and the adsorbed complexes of TMP onto these sites.

the highest steric strains of the [AlO_3] moiety, with the Si–O–Al angles close to 120.0°. Accordingly, the P lone pairs of TMP can easily fill the Al unoccupied orbitals, resulting in an enhanced Lewis acid strength. The LI_4 site is an exception, where the Si–O–Al angles approximate 160.0°. The relevant adsorption energies of TMP indicate that the values are larger for the LI_1, LI_2 and LI_3 sites than for the LI_4 site, agreeing with the geometrical analysis. As indicated by the adsorption energies of TMP bound to the Lewis acid sites, the acid strength decreases in the order of $LI_1 > LI_2 > LI_3 > LI_4$.

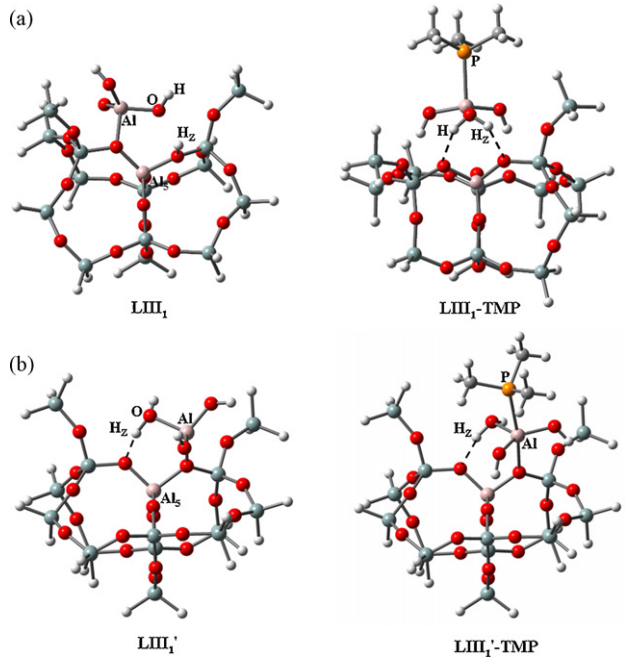

Fig. 9. The B3LYP/6-31G (d, p) optimized geometries for two energy minima (a and b) of the extra-framework $Al(OH)_3$ species ($LIII_1$) of H-Beta zeolite and the adsorbed complexes of TMP onto these sites.

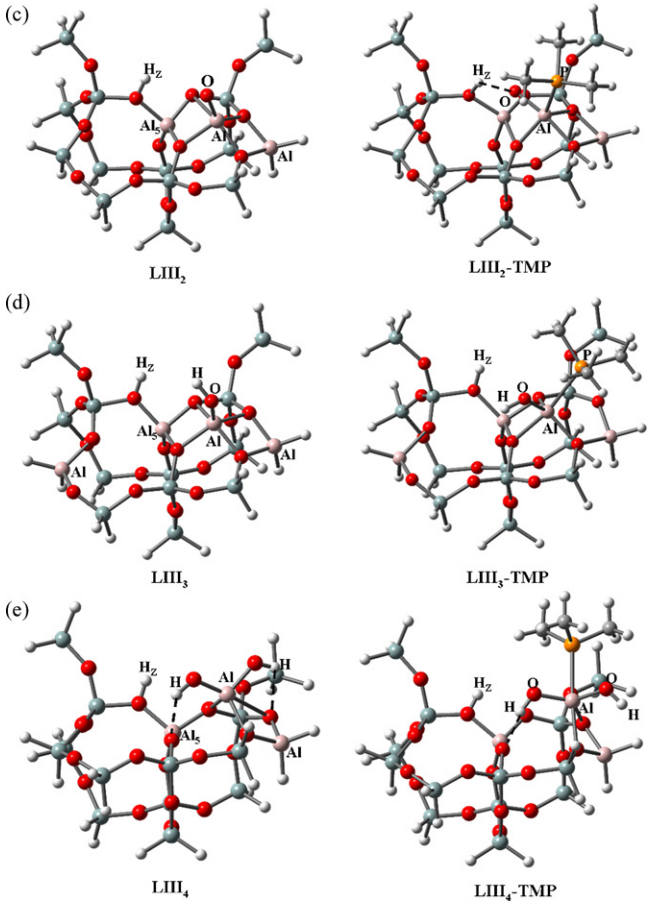

Fig. 10. The B3LYP/6-31G (d, p) optimized geometries for (c) AlO^+ ($LIII_2$), (d) $AlOH^{2+}$ ($LIII_3$) and (e) $Al(OH)_2^+$ ($LIII_2$) cations of H-Beta zeolite and the adsorbed complexes of TMP onto these sites.

With regard to the extra-framework AlO^+ (LII_1) and $Al(OH)_2^+$ (LII_2) species, the optimized geometries in Fig. 8 demonstrate that the AlO^+ and $Al(OH)_2^+$ cations prefer to stay nearby the AlO_4^- tetrahedron, consistent with the structures of the EFAL monovalent cations on H-form Y zeolite [29]. The AlO^+ fragment of the LII_1 species falls within the same plane with the two lattice-O atoms near the framework Al atom. The Al–O distance of 1.882 Å in the coordination complex is longer than the framework Al–O_z distances (1.735 Å). The TMP molecule attacks the AlO^+ center from the top. It results in the formation of a Al–P bond (2.442 Å) and meanwhile changes the Al geometry from trigonal to tetrahedral. The binding energy of TMP adsorbed on the AlO^+ species is close to that of the LI_4 species. As to the $Al(OH)_2^+$ species (LII_2), it also preferentially bi-coordinates with the O atoms near the framework Al. However, the structure of TMP adsorbed on the $Al(OH)_2^+$ species is quite different from that on the AlO^+ species. Instead of the formation of direct Al–P bond, only a weak hydrogen bond occurs between the P atom and the terminal hydroxyl group of the $Al(OH)_2^+$ species. The P–H hydrogen bond distance is optimized at 2.432 Å. The calculated adsorption energy equals to −5.0 kcal mol^{-1} and is characteristic of physisorption.

Two possible structures of $Al(OH)_3$ species ($LIII_1$) having synergistic interplays with the Brønsted acid site, are given in Fig. 9a and b. As shown in Fig. 9a, a direct bond is formed between the $Al(OH)_3$ species and the lattice-O atom. The extra-framework Al atom attains a tetrahedral configuration close to that of the framework Al atom, but the Al–O distances in the complex approximate 2.083 Å and are much longer than those of the framework Al–O_z bonds (ca. 1.745 Å). No hydrogen bond interaction occurs between

the Brønsted acid site (H_z) and $Al(OH)_3$ species. When the TMP molecule is adsorbed on the $Al(OH)_3$ species, the acid proton is transferred to one of the O atoms of the $Al(OH)_3$ species and the EFAL species interacts with two-lattice O atoms near framework Al via two hydrogen bonds. The resultant Al–P bond length is 2.431 Å and the adsorption energy is larger than those previously discussed (-47.9 kcal mol^{-1}). Fig. 9b shows another stable minima for the EFAL $Al(OH)_3$ species. A strong hydrogen bond is formed with the Brønsted acid site. The zeolite hydroxyl O–H_z bond was elongated to 1.494 Å, and the acid proton has been transferred to one O atom of the EFAL $Al(OH)_3$ species. It should produce a remarkable effect on the ^{1}H chemical shift, which was, however, not observed by our previous ^{1}H MAS NMR spectra [42]. Accordingly, the structure of Fig. 9a instead of b is the preferred form of the $Al(OH)_3$ species in dealuminated H-Beta zeolite.

Fig. 10d displays the optimized geometries of the oxo-$AlOH^{2+}$ species ($LIII_3$) in close proximity to the Brønsted acid site. In this case, the EFAL species is located above the five-membered ring compensated by two additional framework Al atoms. As deduced from the Al–O distances in the $AlOH^{2+}$ complex (1.983, 1.956, 1.957 and 1.867 Å), the EFAL cation in tetra-coordination with the lattice O atoms is preferred. In recent ^{27}Al MQ MAS NMR characterizations of the non-hydrated zeolite HY [43], Jiao et al. found the appearance of the ^{27}Al NMR signal at about 35.0 ppm and attributed it to the extra-framework $AlOH^{2+}$ cation in the five-fold oxygen coordination. Furthermore, no hydrogen bonding is formed between the $AlOH^{2+}$ hydroxyl and the framework AlO_4^- tetrahedron. The unperturbed $AlOH^{2+}$ hydroxyl is responsible for the resonances at ca. 0 to -1.0 ppm in ^{1}H MAS NMR spectra [42]. When TMP is directly attached to the $AlOH^{2+}$ species, the O–H_z bond length remains almost unchanged. However, the elongations of the Al–O distances in the coordination complex (1.930, 2.948, 2.055 and 1.885 Å) are observed due to the steric hindrance of TMP suffering from the cluster edges, which can be deduced from the longer Al–P bond of 2.514 Å and a lower adsorption energy of -6.9 kcal mol^{-1}. In the case of the $LIII_2$ site (Fig. 10c), the oxo-AlO^+ species occupy a position on the five-membered ring containing one additional framework Al atom. The calculated Al–O bond lengths in the AlO^+ complex are 2.763, 1.939, 2.066 and 1.885 Å, respectively. Upon the adsorption of TMP on the AlO^+ species, a hydrogen bond of 1.694 Å is formed between the Al=O ligand and the acid proton (H_z), which causes dramatic distortions of the ring structure and elongations in Al–O distances (3.342, 1.884, 1.927 and 1.937 Å, respectively). The adsorption energy is estimated to be -36.3 kcal mol^{-1}. The structure of the $Al(OH)_2^+$ species ($LIII_4$) interacting with the Brønsted acid center is displayed in Fig. 10e. A tetra-coordinated interaction is preferred for this EFAL cation, which is positioned above the five-membered ring. In addition, the hydrogen bonding is formed between the $Al(OH)_2^+$ hydroxyls and lattice-O atoms, consistent with the low-field signal at ca. 2.4 ppm in ^{1}H MAS NMR spectra [42]. The adsorption of TMP on the $Al(OH)_2^+$ species leads to the formation of Al–P bond at 2.533 Å. As expected, the geometry of the cluster experiences a dramatic change upon TMP adsorption as reflected from the increased Al–O distances. The adsorption energy is estimated to be -15.9 kcal mol^{-1}.

The ^{31}P isotropic chemical shifts are calculated for TMP adsorption on all the Lewis acid sites and the data are given in Table 4. The calculated ^{31}P chemical shifts can be resolved into three types. The first includes -48.9, -48.8, -49.5, -50.2, -46.9, -46.1 and -45.0 ppm, corresponding to the adsorption of TMP on the LI_1, LI_2, LI_3, LI_4, $LIII_1$, $LIII_2$ and $LIII_4$ sites, respectively. This type of Lewis acid site is ascribed to the experimental value at -47.0 ppm. Furthermore, the strong ^{31}P–^{27}Al TRAPDOR effect of the -47.0 ppm resonance is evidenced by the formation of direct Al–P bonds in these complexes. The second includes -55.5 and -55.8 ppm for the LII_1 and LII_2 species, which are in reasonable agreement with the experimental signal at -60.0 ppm. No direct Al–P bond is formed on the LII_2 site, consistent with the ^{31}P–^{27}Al TRAPDOR results. Owing to the absence of the ^{31}P–^{27}Al TRAPDOR effect, the ^{31}P NMR peak at -60.0 ppm is probably caused by the physisorption of TMP at the LII_2 site, and the presence of the LII_1 site can be excluded in H-Beta zeolite. The ^{31}P chemical shift for TMP interacting on the $LIII_3$ site is predicted at -35.2 ppm, which is tentatively assigned to the experimental resonance at -32.0 ppm. However, no close proximity of TMP molecule to the Al atom is found for this chemical shift as revealed by our ^{31}P–^{27}Al TRAPDOR spectra, which might be caused by the large QCC of the $LIII_3$ site as proposed by Kao et al. [17] and further investigations are needed to resolve the nature of this Lewis acid site.

Table 4
The B3LYP/6-31G (d, p) geometries and adsorption energies (E_{ads}) for TMP adsorbed on the Lewis acid sites of H-Beta zeolite as well as the ^{31}P chemical shifts obtained at B3LYP/6-31G (d, p) and HF/DZVP2 levels of theory (δ_{cal}) and from ^{31}P MAS NMR experiments (δ_{exp}).

Lewis acids	P–Al (Å)	E_{ads} (kcal mol^{-1})	δ_{cal} (ppm)	δ_{exp} (ppm)
LI_1	2.428	−37.7	−48.9 (−39.6)[b]	
LI_2	2.428	−36.8	−48.8	
LI_3	2.435	−36.5	−49.5	−47.0
LI_4	2.437	−27.6	−50.2	
LII_1	2.442	−28.0	−55.5 (−43.4)	−60.0
LII_2	2.432[a]	−5.0	−55.8 (−57.3)	
$LIII_1$	2.431	−47.9	−46.9	−47.0
$LIII'_1$	2.502	−13.3	−45.3	
$LIII_2$	2.449	−36.9	−46.1	
$LIII_3$	2.514	−6.9	−35.2	−32.0
$LIII_4$	2.533	−15.0	−45.2	−47.0

[a] The P–H distance (see Fig. 8).
[b] The ^{31}P chemical shifts obtained at HF/DZVP2 level of theory.

The HF/DZVP2 method is also employed to predict the ^{31}P chemical shifts for TMP adsorption on several selected Lewis acid sites. The large discrepancies between the experimental and the HF calculated chemical shifts suggest that the DFT method rather than the HF method is superior to predict the ^{31}P chemical shifts on the Lewis acid sites of zeolites.

5. Conclusions

The ^{31}P MAS NMR, ^{31}P–^{27}Al TRAPDOR NMR experiments and theoretical calculations at various levels were combined to study the Brønsted and Lewis acids in H-Beta zeolite, using TMP and TMPO as the probe molecules. The main findings were given below.

Owing to the narrow chemical shift range and close Brønsted acid strengths, the TMP molecules adsorbed at different Brønsted acid sites will undergo fast exchanges and thus only an average peak at -4.5 ppm was observed in ^{31}P MAS NMR spectra. This peak was caused by the transfer of the Brønsted acid protons to the TMP molecules forming the ionized TMP ($TMPH^+$), which was confirmed by the calculated ^{31}P chemical shifts. Three types of Lewis acids were identified and correspond to the ^{31}P MAS NMR peaks at -32.0, -47.0 and -60.0 ppm, respectively. The ^{31}P–^{27}Al TRAPDOR experiments further revealed that the ^{31}P resonance at -47.0 ppm has strong effect and should be caused by the direct Al and P interactions.

The two-layer ONIOM scheme was used to determine the acid proton positions in H-Beta zeolite modeled by a large 32 T cluster, and the links with the acid protons at Al_6–OH–Si_4, Al_1–OH–Si_3 and Al_8–OH–Si_3 sites were preferred. The substitution energies and proton affinities of the three acid sites were found to be close to each other. In addition, the TMP molecules were adsorbed on the 9 T cluster models of three distinct Brønsted acids, and the adsorption energies and chemical shifts were calculated to be close for these Brønsted acid centers. It indicated that the Brønsted acids in H-Beta

zeolite change slightly from site to site and TMP is unable to reflect the subtle differences. Instead, two types of Brønsted acid sites were distinguished by TMPO. The HF/DZVP2 (MP2/DZVP2) chemical shifts of TMPO/H-Beta zeolite were calculated at 68.1 (69.5) and 69.7–72.1 (71.7–74.9) ppm, respectively. The down-field signal at 71.3 ppm can be attributed to TMPO adsorption on either the Al_1–OH–Si_3 or Al_6–OH–Si_4 site, whereas the signal at 67.3 ppm was due to TMPO attached to the Al_8–OH–Si_3 site.

Various types of Lewis acid sites were designed in H-Beta zeolite and the calculated ^{31}P chemical shifts of the TMP adsorption complexes were found to agree well with the experimental results. The three-fold coordinated lattice-Al species, and the extra-lattice oxo-Al species interacting with the Brønsted acid sites such as $Al(OH)_3$, AlO^+ and $Al(OH)_2^+$ will give rise to the ^{31}P MAS NMR resonance at −47.0 ppm. The $Al(OH)_3$ species prefers a mono-coordination with the lattice-O atom, whereas the AlO^+ and $Al(OH)_2^+$ cations are in tetra-coordination with lattice O atoms and occupy the positions nearby the centers of the five-membered ring. It is noteworthy that the strong ^{31}P–^{27}Al TRAPDO effect of the −47.0 ppm resonance was evidenced by the formation of direct Al–P bonds in these cases. The ^{31}P MAS NMR peak at −32.0 ppm was probably caused by TMP adsorption on the extra-lattice $AlOH^{2+}$ species located above the plane of the five-membered ring, whose nature needs further investigations. The peak at −60.0 ppm was conventionally assigned to the TMP physisorption, but our calculations indicated the EFAL monovalent $Al(OH)_2^+$ cation coordinated with two lattice-O atoms near the framework Al atom can contribute to it as well. The TMP molecules were adsorbed through the formation of weak hydrogen bonds.

Acknowledgments

We gratefully acknowledge the financial support of the National Natural Science Foundation of China (grants 20403017 and 20873140) and the Ministry of Science and Technology of China through the National Key Project of Fundamental Research (grant 2009CB623507).

References

[1] J.M. Newsam, M.M. Treacy, W.T. Keotiser, C.B.D. Gruyter, Proc. R. Soc. Lond. A A420 (1988) 375.
[2] X.J. Li, W.P. Zhang, S.L. Liu, L.Y. XU, X.W. Han, X.H. Bao, J. Phys. Chem. C (2008) 5955.
[3] B.L. Su, V. Norberg, Zeolites 19 (1997) 65.
[4] I. Kiricsi, C. Flego, G. Pazzuconi, W.O. Parker Jr., R. Millini, C. Perego, G. Bellussi, J. Phys. Chem. 98 (1994) 4627.
[5] M. Maache, A. Janin, J.C. Lavalley, J.F. Joly, E. Benazzi, Zeolites 13 (1993) 419.
[6] A. Corma, M.I. Juanrajadell, J.M. Lopeznieto, A. Martinez, C. Martinez, Appl. Catal. A 119 (1994) 83.
[7] L. Bonettol, M.A. Camblor, A. Corma, J. Perezpariente, Appl. Catal. A 82 (1992) 37.
[8] J. Limtrakul, Chem. Phys. 193 (1995) 79.
[9] A. Poppl, T. Rudolf, D. Michel, J. Am. Chem. Soc. 120 (1998) 4879.
[10] P.A. Jacobs, H.K. Beyer, J. Phys. Chem. 83 (1979) 1174.
[11] R.D. Shannon, K.H. Gardner, R.H. Staley, G. Bergeret, P. Gallezot, A. Auroux, J. Phys. Chem. 89 (1985) 4778.
[12] S.H. Li, S.J. Huang, W.L. Shen, H.L. Zhang, H.J. Fang, A.M. Zheng, S.B. Liu, F. Deng, J. Phys. Chem. C 112 (2008) 14486.
[13] D. Ma, F. Deng, R. Fu, X. Han, X. Bao, J. Phys. Chem. B 105 (2001) 1770.
[14] F. Collignon, P.A. Jacobs, P. Grobet, G. Poncelet, J. Phys. Chem. B 105 (2001) 6812.
[15] S.B. Hong, S.J. Kim, Y.S. Uh, J. Am. Chem. Soc. 118 (1996) 8102.
[16] J.C. Jansena, E.J. Creyghtonb, S. Lan Njoa, H. van Koningsveld, H.V. Bekkuma, Catal. Today 38 (1997) 205.
[17] H.M. Kao, C.Y. Yu, M.C. Yeh, Micropor. Mesopor. Mater. 53 (2002) 1.
[18] H.M. Kao, C.P. Grey, Chem. Phys. Lett. 259 (1996) 459.
[19] J.H. Lunsford, P.N. Tutunjian, P.J. Chu, E.B. Yeh, D.J. Zalewsk, J. Phys. Chem. 93 (1989) 2590.
[20] J.H. Lunsford, W.P. Rothwell, W.X. Shent, J. Am. Chem. Soc. 107 (1985) 1540.
[21] E.F. Rakiewicz, A.W. Peters, R.F. Wormsbecher, J. Phys. Chem. B 102 (1998) 2890.
[22] J.P. Osegovic, R.S. Drago, J. Phys. Chem. B 104 (2000) 147.
[23] G. Yang, X.J. Lan, J.Q. Zhuang, D. Ma, L.J. Zhou, X.C. Liu, X.W. Han, X.H. Bao, Appl. Catal. A 337 (2008) 58.
[24] C.P. Grey, A.J. Vega, J. Am. Chem. Soc. 117 (1995) 8232.
[25] J. Guan, G. Yang, D.H. Zhou, W.P. Zhang, X.C. Liu, X.W. Han, X.H. Bao, Catal. Commun. 9 (2008) 2213.
[26] J. Guan, G. Yang, D.H. Zhou, W.P. Zhang, X.C. Liu, X.W. Han, X.H. Bao, J. Mol. Catal. A: Chem. 300 (2009) 41.
[27] G. Valerio, A. Goursot, R. Vetrivel, O. Malkina, V. Malkin, D.R. Salahub, J. Am. Chem. Soc. 120 (1998) 11426.
[28] G. Yang, J.Q. Zhuang, D. Ma, X.J. Lan, L.J. Zhou, X.C. Liu, X.W. Han, X.H. Bao, J. Mol. Struct. 882 (2008) 24.
[29] D.L. Bhering, A. Ramírez-Solís, C.J.A. Mota, J. Phys. Chem. C 107 (2003) 4342.
[30] C.J.A. Mota, D.L.N.R. Bhering Jr., Angew. Chem. Int. Ed. 43 (2004) 3050.
[31] S.H. Li, A.M. Zheng, Y.C. Su, H.L. Zhang, L. Chen, J. Yang, C.H. Ye, F. Deng, J. Am. Chem. Soc. 129 (2007) 11161.
[32] M.J. Frisch, G.W. Trucks, H.B. Schlegel, G.E. Scuseria, M.A. Robb, J.R. Cheeseman, V.G. Zakrzewski, J.A. Montgomery, R.E. Stratmann, J.C. Burant, S. Dapprich, J.M. Millam, A.D. Daniels, K.N. Kudin, M.C. Strain, O. Farkas, J. Tomasi, V. Barone, M. Cossi, R. Cammi, B. Mennucci, C. Pomelli, C. Adamo, S. Clifford, J. Ochterski, G.A. Petersson, P.Y. Ayala, Q. Cui, K. Morokuma, D.K. Malick, A.D. Rabuck, K. Raghavachari, J.B. Foresman, J. Cioslowski, J.V. Ortiz, B.B. Stefanov, G. Liu, A. Liashenko, P. Piskorz, I. Komaromi, R. Gomperts, R.L. Martin, D.J. Fox, T. Keith, M.A. Al-Laham, C.Y. Peng, A. Nanayakkara, C. Gonzalez, M. Challacombe, P.M.W. Gill, B.G. Johnson, W. Chen, M.W. Wong, J.L. Andres, M. Head-Gordon, E.S. Replogle, J.A. Pople, Gaussian98 (Revision A.9), Gaussian, Inc., Pittsburgh, PA, 1998.
[33] F. Maseras, K. Morokuma, J. Comp. Chem. 16 (1995) 1170.
[34] M. Gee, R.E. Wasylishen, K. Eichele, J.F. Britten, J. Phys. Chem. A 104 (2000) 4598.
[35] M. Kaupp, O.L. Malkina, V.G. Malkin, J. Comp. Chem. 20 (1999) 91.
[36] A.M. Zheng, L. Chen, J. Yang, M.J. Zhang, Y.C. Su, Y. Yue, C.H. Ye, F. Deng, J. Phys. Chem. B 109 (2005) 24273.
[37] R. Ditchfield, Mol. Phys. 27 (1974) 789.
[38] K. Wolinski, J.F. Hinton, P. Pulay, J. Am. Chem. Soc. 112 (1990) 8251.
[39] J.F. Haw, J.H. Zhang, K. Shimizu, T.N. Venkatraman, D.P. Luigi, W.G. Song, D.H. Barich, J.B. Nicholas, J. Am. Chem. Soc. 122 (2000) 12561.
[40] I. Papai, A. Goursot, F. Fajula, J. Weber, J. Phys. Chem. 98 (1994) 4654.
[41] A.M. Zheng, H.L. Zhang, X. Lu, S.B. Liu, F. Deng, J. Phys. Chem. B 112 (2008) 4496.
[42] X.J. Li, W.P. Zhang, S.L. Liu, X.W. Han, L.Y. Xu, X.H. Bao, J. Mol. Catal. A: Chem. 250 (2006) 94.
[43] J. Jiao, J. Kanellopoulos, W. Wang, S.S. Ray, H. Foerster, D. Freudeb, M. Hunger, Phys. Chem. Chem. Phys. 7 (2005) 3221.